The 2010 IEEE/RSJ International Conference on
Intelligent Robots and Systems
October 18-22, 2010, Taipei, Taiwan

Attitude estimation and control of a quadrocopter

Frank Hoffmann, Niklas Goddemeier, Torsten Bertram
Department of Electrical Engineering and Information Technology
Technische Universität Dortmund
44221 Dortmund, Germany
{frank.hoffmann,niklas.goddemeier,torsten.bertram}@tu-dortmund.de

***Abstract*— The research interest in unmanned aerial vehicles (UAV) has grown rapidly over the past decade. UAV applications range from purely scientific over civil to military. Technical advances in sensor and signal processing technologies enable the design of light weight and economic airborne platforms. This paper presents a complete mechatronic design process of a quadrotor UAV, including mechanical design, modeling of quadrotor and actuator dynamics and attitude stabilization control. Robust attitude estimation is achieved by fusion of low-cost MEMS accelerometer and gyroscope signals with a Kalman filter. Experiments with a gimbal mounted quadrotor testbed allow a quantitative analysis and comparision of the PID and Integral-Backstepping (IB) controller design for attitude stabilization with respect to reference signal tracking, disturbance rejection and robustness.**

I. Introduction

Recent advances in battery, sensor and signal processing technology allow the construction of small sized and light weight UAVs at affordable costs. Thus many researchers explore novel opportunities and applications of UAVs and solve challenges in design, control and autonomous navigation. This paper presents a systematic model based approach to the mechatronic design of an UAV research platform with quadrotor kinematics.

The mechatronic design involves the selection of sensors and actuators, their mounting within the airframe, signal processing and attitude stabilization. The quadrotor dynamics are derived either in terms of the Euler-Lagrange formalism [1], [2] or by means of Newton-Euler equations [3], [4], [5] which form the basis of our model. In addition the complete mechatronic model captures the rotor and motor dynamics and sensors to enable realistic simulations of the state estimator and closed loop behavior. The UAV motion is observed by means of a customary designed low-cost MEMS inertial measurement unit (IMU) composed of three gyroscopes and a three axis accelerometer. The raw sensor signals are filtered and fused by a Kalman filter to estimate attitude and position. The attitude stabilization controllers are based on a conventional PID controller and an integral backstepping controller design [6] operating at a sample rate of 100Hz. Both controllers are analyzed with respect to robustness and disturbance rejection.

In contrast to a classical helicopter with main and tail rotor a quadrocopter is propelled by four horizontal rotors directly attached to the airframe. In case of small size quadrocopters the rotor pitch is fixed which renders a swashplate obsolete. The quadrocopter motion is controlled by the thrust generated by individual propellers regulated by the motor velocity.

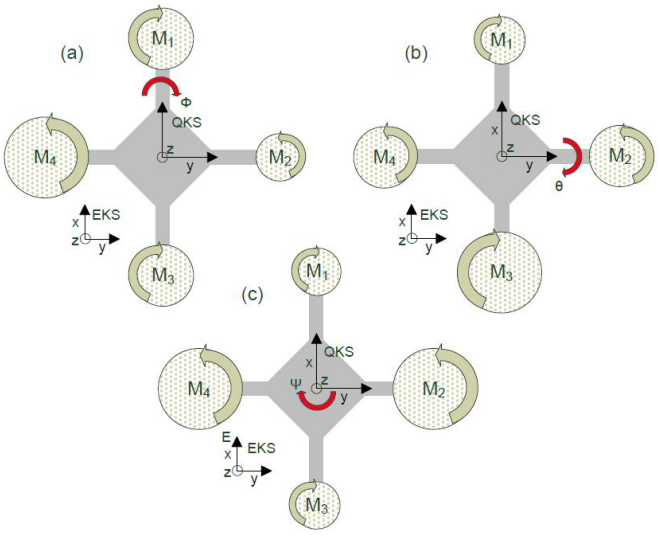

Fig. 1: Quadrocopter frame with propeller and rotor velocity configurations

Fig. 1 illustrates the quadrocopter body frame and the external frame, the location of propellers and combination of rotor velocities to independently generate roll (a), pitch (b) and yaw (c) motion. Translational motion is generated by an offset in roll and pitch. The flight altitude is controlled by the total thrust produced by all four rotors. The quadrocopters six degrees of freedom are controlled by the four motors resulting in an underactuated system. Conventional quadrocopter control design relies on a nested control loop, in which the inner loop achieves attitude stabilization and the outer loop regulates the translational motion.

II. Mechatronic design

An extra payload of about 200–300 g is required to equip the quadrocopter with vision and additional sensors. With standard off-the-shelf components, a light weight airframe and a lithium-polymer accumulator the total weight of platform amounts to about 600 g. Considering a safety margin and sufficient agility demands a thrust weight ratio of about $2:1$, which requires each motor to generate about 450 g of thrust. The actuators are brushless motors controlled by separate motor drivers with pulse width modulation (PWM) and

inter-integrated circuit (I^2C) interface. The I^2C interface offers the advantage of a high clock rate of motor commands and the ability to monitor the motor status in terms of motor speed, current and temperature.

The attitude is estimated by integrating the angular velocities measured by three gyroscopes along the three axis of rotation. In order to compensate the long term drift a three axis accelerometer determines the absolute orientation of gravitation. The IMU is mounted in the center of rotation to obtain unbiased observations.

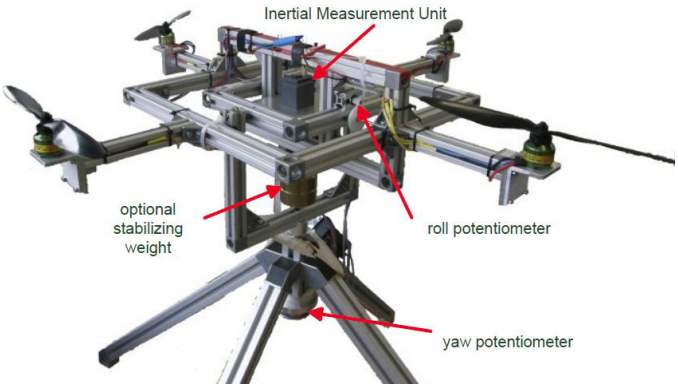

Fig. 2: Quadrocopter test bench

The IMU is attached to a gimbal with three rotational degrees of freedom actuated by the four rotors as shown in Fig. 2. The gimbal axes are equipped with potentiometers which provide the ground truth of the platforms absolute orientation in terms of pitch, roll and yaw. The gimbal mounting in conjunction with the orientation encoders allows a systematic validation and comparison of state estimators and alternative controller designs. In addition it enables safe development and evaluation of sensing, signal processing and control with hardware-in-the-loop. Safe evaluation under realistic conditions is essential in quadrocopter development as in contrast to a conventional two rotor helicopter human manual teleoperated control of the quadrotor is impossible without attitude stabilization. The motors operate at speeds that generate the nominal thrust. The noise induced by motor vibrations on the IMU is considered in the Kalman filter design. The experimental platform also allows a reproducible and quantitative evaluation of the robustness of the controller by adding or shifting mass and disturbance rejection e.g. the response to wind gusts.

III. System Modeling and Identification

The dynamic model describes the translational and rotational motion in response to the thrust generated by the four rotors. The model parameters of the test bench are obtained by an open-loop step response analysis and are identified with a least-square method.

A. Quadrocopter model

The dynamic model is divided into a translational and a rotational part. The translational part (1) describes the motion generated by forces acting on the body frame.

$$\begin{bmatrix} m & 0 & 0 \\ 0 & m & 0 \\ 0 & 0 & m \end{bmatrix} \cdot \begin{bmatrix} \ddot{X} \\ \ddot{Y} \\ \ddot{Z} \end{bmatrix} - \begin{bmatrix} 0 \\ 0 \\ mg \end{bmatrix} = \mathbf{R}_Q^E \cdot \mathbf{T}^Q \qquad (1)$$

$\mathbf{R}_Q^E$ is the direct-cosine matrix which transforms forces $\mathbf{T}^Q$ acting in the body frame Q to the global reference frame with coordinates $[X, Y, Z]^T$. The earth gravity constant is denoted with g, m represents the quadrocopter mass. The rotational dynamics take two gyroscopic effects into account. The more significant gyroscopic effect is caused by the propeller rotation which tends to stabilize the quadrocopter along its horizontal axis:

$$M_{R_x} = -J_R \dot{\theta} \Omega, M_{R_y} = J_R \dot{\phi} \Omega \qquad (2)$$

in which J_R denotes the rotor inertia and Ω the propeller angular velocity. The second effect emerges from the rotation of the platform itself. These rotations are comparatively slow and are thus derived from angular momentum theory. The torque is defined as $\mathbf{M} = \dot{\mathbf{L}}$ in which $\mathbf{L}$ denotes the angular momentum with $\mathbf{L} = \mathbf{I}\omega$, $\mathbf{I}$ denotes the inertial matrix and ω the angular velocity of the body. Combining both gyroscopic effects the rotational dynamics are described by:

$$\begin{bmatrix} I_x \ddot{\phi} \\ I_y \ddot{\theta} \\ I_z \ddot{\psi} \end{bmatrix} = \begin{bmatrix} \dot{\psi}\dot{\theta}(I_y - I_z) \\ \dot{\psi}\dot{\phi}(I_z - I_x) \\ \dot{\theta}\dot{\phi}(I_x - I_y) \end{bmatrix} + \begin{bmatrix} -J_R \dot{\theta} \Omega \\ J_R \dot{\phi} \Omega \\ 0 \end{bmatrix} + \begin{bmatrix} M_\phi \\ M_\theta \\ M_\psi \end{bmatrix} \qquad (3)$$

with

$$\begin{aligned} M_\phi &= l(T_4 - T_2) \\ M_\theta &= l(T_1 - T_3) \\ M_\psi &= d(T_2 + T_4 - T_1 - T_3) \end{aligned} \qquad (4)$$

in which T_i denotes the thrust generated by propeller i, l is the distance between the propeller axis and the center of gravity and d denotes a thrust to torque coefficient depending on the propeller blade geometry. The complete model of the quadrocopter is given by:

$$\begin{aligned} \ddot{X} &= (\cos\phi \sin\theta \cos\psi + \sin\phi \sin\psi) \sum_i T_i/m \\ \ddot{Y} &= (\cos\phi \sin\theta \sin\psi - \sin\phi \cos\psi) \sum_i T_i/m \\ \ddot{Z} &= mg + (\cos\phi \cos\theta) \sum_i T_i/m \\ \ddot{\phi} &= \dot{\psi}\dot{\theta}(\frac{I_y - I_z}{I_x}) - \frac{J_R}{I_x}\dot{\theta}\Omega + \frac{1}{I_x} M_\phi \\ \ddot{\theta} &= \dot{\psi}\dot{\phi}(\frac{I_z - I_x}{I_y}) + \frac{J_R}{I_y}\dot{\phi}\Omega + \frac{1}{I_x} M_\theta \\ \ddot{\psi} &= \dot{\phi}\dot{\theta}(\frac{I_x - I_y}{I_z}) + \frac{1}{I_x} M_\psi \end{aligned} \qquad (5)$$

The translational part is referenced in a fixed global reference frame whereas the rotational part is described in quadrocopter centric coordinates.

B. Gimbal test bench model

The model of the gimbal mounted test bench is similar to the rotational part of (5), except for two additional terms that capture the rotation of the gimbal mounting. The ball bearings on each axis cause friction terms r_ϕ, r_θ, r_ψ into (3) defined by

$$r_\phi = b_\phi \dot{\phi}, r_\theta = b_\theta \dot{\theta}, r_\psi = b_\psi \dot{\psi} \tag{6}$$

in which $b_{\phi,\theta,\psi}$ denote the friction coefficients.

Additional weights for stabilization can be attached underneath the body frame. These weights are helpful for initial tests of the attitude stabilization as the non-actuated platform is inherently stable. Reduction of the weights gradually reduces and eventually cancels this self-stabilization. Under the assumption of small deviations from the vertical orientation the weights act like a pendulum with restoring forces $F_{r\phi}$ and $F_{r\theta}$ with

$$F_{r_\phi} = k_\phi \phi, F_{r_\theta} = k_\theta \theta \tag{7}$$

in which k_ϕ, k_θ denote the equivalent spring constants. The complete rotational model for the test bench is given by:

$$\begin{bmatrix} I_x \ddot{\phi} \\ I_y \ddot{\theta} \\ I_z \ddot{\psi} \end{bmatrix} = \begin{bmatrix} \dot{\psi}\dot{\theta}(I_y - I_z) \\ \dot{\psi}\dot{\phi}(I_z - I_x) \\ \dot{\theta}\dot{\phi}(I_x - I_y) \end{bmatrix} + \begin{bmatrix} M_{R_x} \\ M_{R_y} \\ 0 \end{bmatrix} - \begin{bmatrix} k_\phi \phi \\ k_\theta \theta \\ k_\psi \psi \end{bmatrix} - \begin{bmatrix} k_\phi \phi \\ k_\theta \theta \\ k_\psi \psi \end{bmatrix} + \begin{bmatrix} M_\phi \\ M_\theta \\ M_\psi \end{bmatrix} \tag{8}$$

Equations (3) and (8) reveal the nonlinear coupling among rotations caused by gyroscopic effects. Due to the small rotational motion the gyroscopic effects can be neglected in comparison with friction and actuator torque resulting in a linear model of a mass-spring-damper system.

C. Actuator model

The actuator is composed of the motor controller, motor and air screw. For the proper design of the attitude controller it is important to determine its static gain and dynamic response. The gain denotes the ratio between the control input to generated thrust and angular momentum. The delay emerges from the acceleration of the propeller in response to change in reference turn rate. Experiments reveal that the relation between control inputs and generated thrust is approximately linear across the regime of useful operation. The identified rising time is about $0.2\,\mathrm{s}$ resulting in a first order transfer function with gain K and time constant T:

$$G_{u_i \to \Omega_i}(s) = \frac{K}{Ts + 1} \tag{9}$$

IV. State Estimation

This section describes the state estimation of the quadrocopter attitude in terms of the three rotations $[\phi, \theta, \psi]^T$ based upon a low-cost IMU. Accelerometers and gyroscopes possess complementary characteristics regarding sample rate and drift. The measurements of turn rate and acceleration are forged by sensor noise and vibrations induced by the rotation of the rotors. The sensor noise is caused by temperature sensitivity, quantization noise and bias instability. A Kalman filter integrates the signals of both sensor types and thus reduces the noise to achieve robust state estimates.

Accelerometers measure the earth gravity vector and thus directly observe roll and pitch angles. However, the signals are highly sensitive to vibrations induced by the propellers. These vibrations disturb the signals by about $\pm 6\,^\circ$, a second order low-pass filter reduces the signal noise to about $\pm 3\,^\circ$ but introduces signal latency.

Gyroscopes measure the angular rates along the rotational axis. The absolute rotation is obtained by integration of the angular rate signals over time. The gyroscopes are less sensitive to the vibrations, however tend to drift. The identification and modeling of the signal noise in terms of the process and measurement covariance is based on the Allan-Variance analysis [7].

The Kalman filter integrates the angular velocities provided by gyroscopes as inputs to predict the absolute orientation. The process is merely an integration and is subject to a drift such that over time the state error grows without bounds. Experiments show that after $100\,\mathrm{s}$ of operation the error amounts to about $10\,^\circ - 20\,^\circ$. The accelerometers provide absolute measurements of the attitude utilized in the correction to compensate for the drift in the prediction. Fig. 3 shows the final $100\,\mathrm{s}$ of an experiment on the test bench under realistic manœuvres and operating conditions. The plot compares the reference, gyro and accelerometer signals and the Kalman filter estimation. Notice, the error drift in the gyro signal and the noise in the accelerometer signal. The

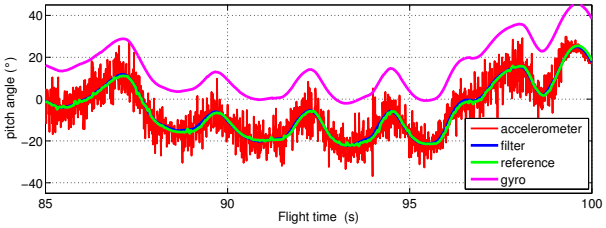

Fig. 3: Kalman-filter state estimate

comparison of the state estimation by the Kalman filter with the ground truth provided by potentiometers on the gimbal mounting shows that the average orientation error amounts to about $1\,^\circ$. The accuracy is fully sufficient for stabilization in consideration of the magnitude of external disturbances acting upon the quadrocopter.

V. Attitude Control

This sections describes a classical PID-controller and an integral backstepping (IB)-controller for attitude stabilization of a quadrocopter. Fig 4 illustrates the overall control architecture composed of a feed-forward altitude compensator and feedback attitude and altitude control. The orientation error $e = \mathbf{w_R} - \mathbf{r}$ is the difference between the reference attitude $\mathbf{w_R}$ and the estimated orientation $\mathbf{r}$. The control input u is the sum of feedback control u_R and feed forward control u_S. The direction of thrust changes with roll and pitch causing

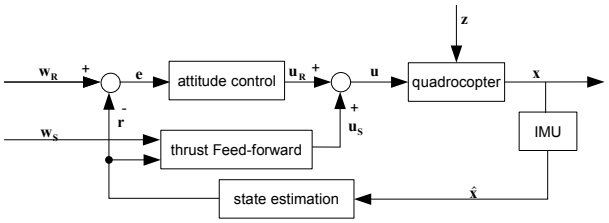

Fig. 4: Control structure

a horizontal motion of the quadrocopter. A quadrocopter tilt reduces the lift to balance the gravity force causing a loss of altitude. The thrust feed-forward compensator counteracts this reduction in effective lift and thus stabilizes the altitude. The attitude controller supports the human teleoperator as an autopilot in that joystick controls are interpreted as attitude reference signals. Alternatively, the attitude controller serves as the inner loop of a position and velocity controller to enable fully autonomous operation.

As mentioned in section III the test bench is described by the decoupled dynamics model without gyroscopic effects in equation (8), thus controllers for the roll, pitch and yaw axis are designed independently.

The initial parameters of the time continuous PID controllers are obtained and optimized in simulation by means of the Ziegler-Nichols method. These parameters are then transfered onto the controller of the test bench. This procedure guarantees an initially stable controller which allows collection of further identification data to refine the model parameters. The initial controller parameters are manually tuned to improve the closed loop response in terms of an optimal compromise between disturbance rejection and reference tracking.

The controllers are analyzed in terms of robustness with respect to model uncertainties, tracking performance on step responses and with respect to disturbance rejection. The reference signal is composed of steps of $15°$ which amounts to about half of the maximum roll and pitch angle. These maximum orientations denote the limits of the flight envelope under normal operation. Furthermore a reference signal is generated by teleoperation with a remote control, the pilot signals emulate realistic flight commands. The disturbance rejection is evaluated by a sequence of impulses added to the control in hovering state which emulate the effect of wind gusts. The robustness of the controller is evaluated by an extra weight mounted to one of the quadrocopters arms to simulate variations in payload and inertia. The closed loop performance is evaluated in simulation as well as experiment using the exact same reference signals and disturbances.

A. PID control

The control law for the PID-Controller is given by:

$$K_{PID}(s) = k_P + k_I \frac{1}{s} + k_D s \tag{10}$$

Initial gains k_P, k_I and k_D in table I are derived by the Ziegler-Nichols method and are then manually tuned with

TABLE I: PID-controller parameters

	P	I	D
roll	0.7	0.3	0.25
pitch	0.8	0.3	0.3
yaw	2	0.3	0.4

respect to reference tracking. The step responses in Fig. 5 illustrate the tracking performance of the PID controller. The rise time for the positive step is $0.8\,\mathrm{s}$ with an overshoot of $1.2\,°$. For the negative step the rise time amounts to $1.1\,\mathrm{s}$

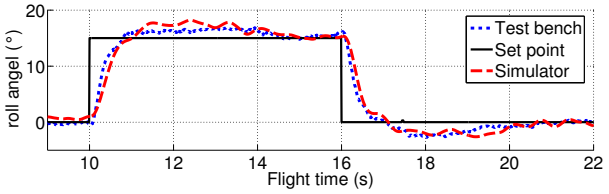

(a) Roll axis step response

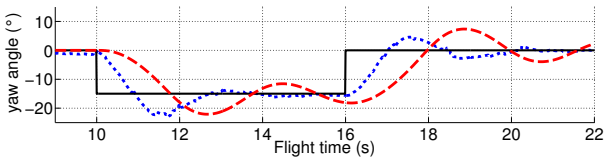

(b) Yaw axis step response

Fig. 5: Step response for a set point of $15\,°$ and $6\,\mathrm{s}$ length.

with an overshoot of $2.3\,°$. For simulation and experiment the rise and settling times are almost identical only the overshoot is about $0.4\,°$ larger in the simulation. The yaw step response shows that the PID parameters are suboptimal causing insufficiently damped oscillations of the closed loop system.

Fig. 6 shows the tracking behavior of the PID controller with respect to pilot attitude reference commands. The average steady state error between pilot command and quadrocopter attitude is $-0.1\,°$ with a standard deviation of $2.34\,°$. This control performance allows the platform to execute agile manœuvres. In case of rapid motions the simulated response is a bit sluggish causing a delay of about $0.45\,\mathrm{s}$.

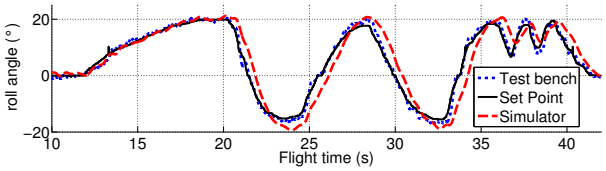

Fig. 6: Tracking behavior of the PID controller

The disturbance rejection is illustrated in Fig. 7 in which at times $9\,\mathrm{s}$, $12.5\,\mathrm{s}$ and $16\,\mathrm{s}$ a disturbance impulse causes an attitude error between $16\,°$ and $25\,°$. The PID controller compensates the induced attitude errors within less than $1\,\mathrm{s}$ with an overshoot of about $6\,°$. The robustness of the controller is evaluated by an extra weight of $90\,\mathrm{g}$ attached to

the tip of a quadrocopters arm at time 20 s and removed at time 32 s. The impulse of the sudden weight change causes an attitude error of about 8 °, the steady state error is compensated within 5 s.

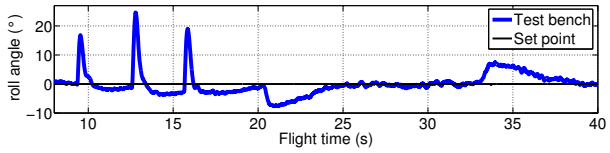

Fig. 7: Disturbance compensation of the PID controller

The experiment shows that the model and identified model parameters are accurate and that the simulation captures the actual dynamics. The PID controller stabilizes the quadrocopter in a robust and efficient manner and exhibits a good compromise between tracking and disturbance compensation.

B. Integral backstepping control

This section describes the development and evaluation of an integral backstepping controller. The derivation of the control law is based on the notation described in [2] and [8].

The control error e_ϕ is defined by the reference ϕ_{Set} and the actual orientation ϕ by

$$e_\phi = \phi_{Set} - \phi \tag{11}$$

The derivative of the control error e_ϕ is given by

$$\dot{e}_\phi = \dot{\phi}_{Set} - \omega_x \tag{12}$$

the angular velocity ω_x is not identical with the control input and is thus defined by a virtual control law

$$\omega_{x_{Set}} = k_1 e_\phi + \dot{\phi}_{Set} + k_2 \int e_\phi \mathrm{dt} \tag{13}$$

This formulation introduces the integral terms into the backstepping design. The parameters k_1 and k_2 are positive gains. The error in ω_x is described by

$$e_{\omega_x} = \omega_{x_{Set}} - \omega_x \tag{14}$$

and by using (13) possesses the derivative:

$$\begin{aligned} \dot{e}_{\omega_x} &= \dot{\omega}_{x_{Set}} - \ddot{\phi} && (15)\\ &= k_1 \dot{e}_\phi + \ddot{\phi}_{Set} + k_2 e_\phi - \ddot{\phi} && (16)\\ &= k_1(\dot{\phi}_{Set} - \omega_x) + \ddot{\phi}_{Set} + k_2 e_\phi - \ddot{\phi} && (17) \end{aligned}$$

Equation (12) can be rewritten using (13) and (14) as:

$$\begin{aligned} \dot{e}_\phi &= \dot{\phi}_{Set} - (k_1 e_\phi + \dot{\phi}_{Set} + k_2 \int e_\phi \mathrm{dt} - e_{\omega_x}) && (18)\\ &= -k_1 e_\phi - k_2 \int e_\phi \mathrm{dt} + e_{\omega_x} && (19) \end{aligned}$$

Using the angular rate $\ddot{\phi}$ and the dynamic model described in equation (3) finally the control input u_2 is introduced:

$$\begin{aligned} \dot{e}_{\omega_x} &= k_1(\dot{\phi}_{Set} - \omega_x) + \ddot{\phi}_{Set} + && (20)\\ & \quad k_2 e_\phi - \dot{\theta}\dot{\psi}\frac{I_y - I_z}{I_x} + \frac{J_R}{I_x}\dot{\theta}\Omega - \frac{1}{I_x}u_2 \end{aligned}$$

Similar to equation (13) the desired dynamics of the angular velocity are governed by:

$$\dot{e}_{\omega_x} = -k_3 e_{\omega_x} - e_\phi \tag{21}$$

This behavior is achieved if the control input satisfies:

$$\begin{aligned} M_\phi &= I_x[(1 - k_1^2 + k_2)e_\phi + (k_1 + k_3)e_{\omega_x} - && (22)\\ & \quad k_1 k_2 \int e_\phi dt + \ddot{\phi}_{Set} - \dot{\theta}\dot{\psi}\frac{I_y - I_z}{I_x} + \frac{J_R}{I_x}\dot{\theta}\Omega] \end{aligned}$$

Using (18) the control law (22) can be transformed into PID-form:

$$\begin{aligned} M_\phi &= I_x[(1 + k_2 + k_1 k_3)e_\phi + (k_1 + k_3)\dot{e}_\phi + && (23)\\ & \quad k_3 k_2 \int e_\phi dt + \ddot{\phi}_{Set} - \dot{\theta}\dot{\psi}\frac{I_y - I_z}{I_x} + \frac{J_R}{I_x}\dot{\theta}\Omega] \end{aligned}$$

The control laws for the pitch and yaw axis are derived in the same manner.

The block diagram of the controller is shown in Fig. 8.

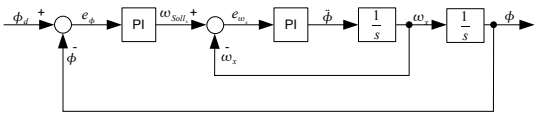

Fig. 8: Block diagram of integral backstepping controller

The IB controller is evaluated in the same set of experiments as the PID controller. The step response of the roll

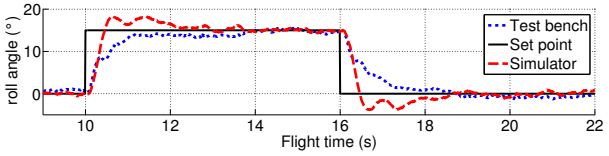

(a) Roll axis step response

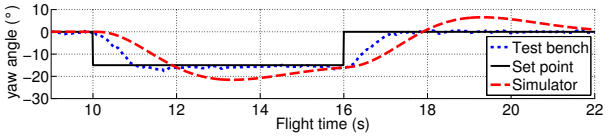

(b) Yaw axis step response

Fig. 9: Step response with amplitude of 15 ° and duration 6 s length.

axis shown in Fig. 9a exhibits a rise time of 0.8 s with an overshoot of 1 °. The yaw control is superior in comparison to the PID controller with a rise time of 1.0 s with an overshoot of 2.3 °. The IB controller achieves even better results comparing the simulation of the yaw step response. In general the attitude behaves more smoothly with IB control compared to PID control.

Fig. 10 shows the reference tracking of the IB controller. The true attitude of the quadrocopter shows a standard deviation of 1.15 ° with respect to the reference trajectory. The simulation exhibits a delay of 0.2 s. The disturbance compensations of the IB controllers are not shown but their performance is similar to the PID controller. The ability to

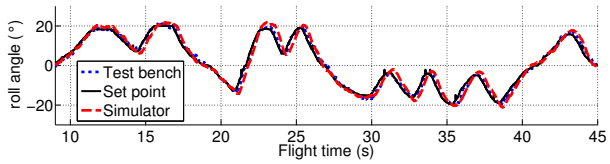

Fig. 10: Tracking integral backstepping controller

cope with wind gusts is tested by exposing the platform to an air flow of about $8\,\mathrm{m/s}$ generated by a wind machine. During this exposure the platform is supposed to track a sinusoidal reference signal along the roll axis with an amplitude of $20\,^\circ$ and a frequency of $170\,^\circ/\mathrm{s}$. To show the effects of the wind a test flight of $50\,\mathrm{s}$ is emulated with an onset of wind between $20\,\mathrm{s}$ and $40\,\mathrm{s}$. Without the wind disturbance the maximum overshoot at the peak amplitudes is about $2\,^\circ$. The wind disturbance increases the overshoot to a maximum of $4\,^\circ$, compare Fig. 11a. The wind has almost no effect on a yaw axis motion as shown in Fig. 11b. The robustness of the

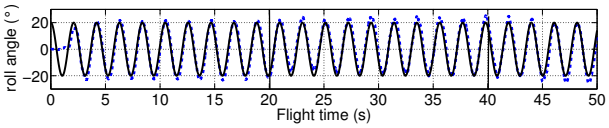

(a) Roll axis wind disturbance

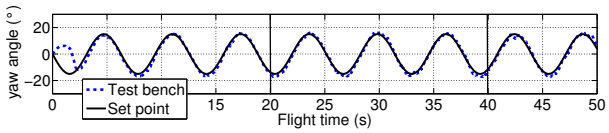

(b) Yaw axis wind disturbance

Fig. 11: Disturbance rejection with respect to wind gusts.

controller is evaluated by an extra weight of $330\,\mathrm{g}$ attached to the top of the quadrocopter which shifts the center of gravity above the center of rotation, increasing the inherent instability of the system. Fig. 12 shows the roll axis step responses and the reference tracking.

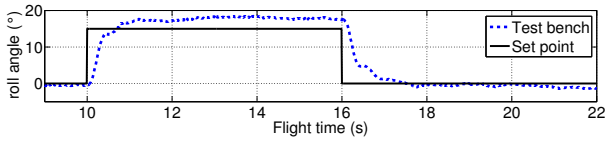

(a) Roll axis step response

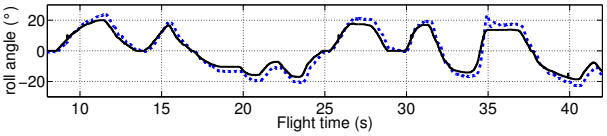

(b) Roll axis tracking

Fig. 12: Robustness with respect to parameter uncertainties.

The rise time of the positive step response is not effected by the additional weight as the torque generated by gravity supports coincides with the turning direction. In case of the negative step the thrust has to compensate the extra gravity torque. Therefore the rise time increases to $1.5\,\mathrm{s}$. The additional weight exhibits a slightly negative effects tracking performance causing a larger overshoot as shown in Fig. 10. The experimental results demonstrate the robustness of the IB controller and its ability to handle parameter uncertainties. The control is stable even under degraded conditions, yet effective to allow agile motions of the quadrocopter.

VI. Conclusions

Systematic modeling, control design and evaluation are crucial for the safe operation of quadrocopter platforms as design errors almost inevitably cause crashes of the quadrocopter. The simulation and experimental verification demonstrate that the proposed control design is suitable for robust but still agile attitude control of a quadrocopter. The hardware in the loop evaluation of attitude stabilization on a gimbal mounting provides confidence in subsequent flight experiments. The attached video shows the disturbance rejection and the tracking of a sinusoidal reference signal under exposure to wind gusts. The model captures the essential dynamics of the quadrocopter and provides the basis for optimal control design. The Kalman filter fuses the accelerometer and gyroscope signals and provides a robust estimation of the quadrocopter attitude with an error of less than $1\,^\circ$. The PID and IB controller stabilize the quadrocopter within the specified flight envelope. The IB controller demonstrates smoother motion and slightly better tracking performance. The IB controller parameters can be transfered into equivalent PID controller gains as both control schemes possess the same basic dynamic structure. The main difference between the two schemes is that the inner loop IB controller directly refers to the gyroscope signals whereas the PID controller refers to the derivative of the attitude error. In addition IB design allows a more transparent specification in terms of desired inner and outer loop dynamics. Future work is concerned with the transfer of the sensors, actuators and signal processing onto a free flying platform.

References

[1] A. Soumelidis, P. Gaspar, G. Regula, and B. Lantos. Control of an experimental mini quad-rotor uav. In *16th Mediterranean Conference on Control and Automation*, pages 1252–1257, June 2008.

[2] S. Bouabdallah. *Design and Control of Quadrotors with application to autonomous flying*. PhD thesis, Ecole Polytechnique Federale De Lausanne, 2007.

[3] B. Erginer and E. Altug. Modeling and PD control of a quadrotor VTOL vehicle. In *IEEE Intelligent Vehicles Symposium*, pages 894–899, June 2007.

[4] G. M. Hoffmann, H. Huang, S. L. Waslander, and C. J. Tomlin. Quadrotor helicopter flight dynamics and control: Theory and experiment. In *AIAA Guidance, Navigation and Control Conference*, 2007.

[5] I. D. Cowling, O. A. Yakimenko, J. F. Whidborne, and A. K. Cooke. A prototype of an autonomous controller for a quadrotor UAV. Technical report, 2007.

[6] H. K. Khalil. *Nonlinear Systems*. Prentice Hall, 2002.

[7] *IEEE Standard Specifcation Format Guide and Test Procedure for Single-Axis Interferometric Fiber Optic Gyros*. IEEE Std 952-1997, 1998.

[8] A.A. Mian and W. Daobo. Nonlinear flight control strategy for an underactuated quadrotor aerial robot. In *IEEE International Conference on Networking, Sensing and Control, ICNSC 2008*, pages 938–942, April 2008.